Ecotoxicology and Environmental Safety 132 (2016) 372–378

Contents lists available at ScienceDirect

Ecotoxicology and Environmental Safety

journal homepage: www.elsevier.com/locate/ecoenv

Graphene oxide induces plasma membrane damage, reactive oxygen species accumulation and fatty acid profiles change in *Pichia pastoris*

Meng Zhang [a], Qilin Yu [a], Chen Liang [a], Zhe Liu [a], Biao Zhang [b], Mingchun Li [a,*]

[a] Ministry of Education, Key Laboratory of Molecular Microbiology and Technology, Department of Microbiology, College of Life Science, Nankai University, Tianjin 300071, PR China

[b] Tianjin Traditional Chinese Medicine University, Tianjin 300193, PR China

ARTICLE INFO

Article history:
Received 26 March 2016
Received in revised form
19 June 2016
Accepted 20 June 2016
Available online 1 July 2016

Keywords:
Graphene oxide
Unsaturated fatty acid
Reactive oxygen species
Membrane damage
Pichia pastoris

ABSTRACT

During the past couple of years, graphene nanomaterials were extremely popular among the scientists due to the promising properties in many aspects. Before the materials being well applied, we should first focus on their biosafety and toxicity. In this study, we investigated the toxicity of synthesized graphene oxide (GO) against the model industrial organism *Pichia pastoris*. We found that the synthesized GO showed dose-dependent toxicity to *P. pastoris*, through cell membrane damage and intracellular reactive oxygen species (ROS) accumulation. In response to these cell stresses, cells had normal unsaturated fatty acid (UFA) levels but increased contents of polyunsaturated fatty acid (PUFA) with up-regulation of UFA synthesis-related genes on the transcriptional level, which made it overcome the stress under GO attack. Two UFA defective strains (*spt23*Δ and *fad12*Δ) were used to demonstrate the results above. Hence, this study suggested a close connection between PUFAs and cell survival against GO.

1. Introduction

Graphene is the name given to a flat monolayer of carbon atoms tightly packed into a two-dimensional (2D) honeycomb lattice, and is a basic building block for graphitic materials of all other dimensionalities (Geim and Novoselov, 2007). Graphene research has been more and more popular because graphene has many characteristics which reach theoretically predicted limits, such as room-temperature electron mobility (Mayorov et al., 2011), high thermal conductivity (Balandin, 2011), optical absorption (Nair et al., 2008), complete impermeability to any gases (Bunch et al., 2008) and readily chemical functionalization (Elias et al., 2009; Nair et al., 2010). The numerous properties make it potentially promising for bioapplications (Novoselov et al., 2012). Before the scientists use it to fulfill its promise in the biomedical area, we must grasp its toxicity to organisms, firstly.

Many studies have demonstrated the toxicity of carbon nanomaterials, such as their acute toxic effects in primary cultures (Belyanskaya et al., 2009), oxidative stress, inflammation (Murray et al., 2009) and plasma membrane damage (Hirano et al., 2008). As with other nanomaterials, graphene nanomaterials lead to direct or indirect generation of intracellular ROS which can interfere with biochemical processes and induce cytotoxicity and genotoxicity (Zhang et al., 2014). Cellular ROS are generated endogenously from the mitochondria or formed with the exogenous sources. Generally, cells own an antioxidant defense system to eliminate free radicals. When excess ROS cannot be cleaned, oxidative stress occurs and results in ROS-mediated damage of many biomolecules, such as nucleic acids, proteins and lipids (Catala, 2012). Previous study showed that followed ROS accumulation by graphene exposure, apoptosis is activated through the MAPK and TGF-β signaling pathways (Li et al., 2012).

As one of the most important molecules in the cell, fatty acids, especially unsaturated fatty acids (UFAs), not only function as energy sources, but also are required for membrane synthesis, and further influence many cell processes, including cell growth and proliferation (Carracedo et al., 2013). The model industrial organism, *Pichia pastoris*, has four fatty acid desaturase (*FAD*) genes, including *FAD9A* and *FAD9B* (encoding Δ-9 desaturase), *FAD12* (encoding Δ-12 desaturase) and *FAD15* (encoding Δ-15 desaturase) and can synthesize three UFAs including oleic acid, linoleic acid and α-linolenic acid (Yu et al., 2012b). UFA synthesis is controlled by a series of desaturation processes with the desaturases above and the *FAD* gene transcription is regulated by a transcriptional factor, Spt23 (Yu et al., 2012a). Compared to the model organism *Saccharomyces cerevisiae* which only synthesizes one kind

Abbreviations: DCFH-DA, 2′,7′-dichlorofluorescein diacetate; FAD, fatty acid desaturase; FAMEs, fatty acid methyl esters; GO, graphene oxide; PI, propidium iodide; PUFA, polyunsaturated fatty acid; ROS, reactive oxygen species; UFA, unsaturated fatty acid

* Correspondence to: Department of Microbiology, College of Life Science, Nankai University, Tianjin 300071, PR China.
E-mail address: nklimingchun@163.com (M. Li).

http://dx.doi.org/10.1016/j.ecoenv.2016.06.031
0147-6513/

of UFA (oleic acid), *P. pastoris* possesses a relatively complete system of UFA biosynthesis which can provide the evidence of the relationship between UFAs and the membrane damage induced by GO more fully. According to the reasons above, *P. pastoris* is an appropriate eukaryotic model organism for toxicity investigation of graphene nanomaterials associated with fatty acid synthesis and membrane damage.

In this study, we for the first time investigated the effect of synthesized graphene oxide (GO) on *P. pastoris*, and discussed the possible toxicity mechanisms of these nanomaterials to this model organism. Our results revealed that the graphene nanomaterials showed dose-dependent toxicity to *P. pastoris*. Moreover, we found the toxicity was mainly due to membrane damage and cellular ROS accumulation which may be overcome by increasing PUFA synthesis.

2. Materials and methods

2.1. Synthesis and characterization of graphene oxide (GO)

GO used in this study was synthesized by the modified Hummer's method (Hummers Jr and Offeman, 1958). Transmission electron microscopy was performed to observe the GO structure with a transmission electron microscope (TEM, Tecnai G2 F-20, FEI, USA). A Raman spectroscopy (Renishaw inVia, England) was used to examine the characteristic Raman shift of GO.

2.2. Preparation of GO solutions

10 mg of the GO were suspended in 1 mL SC medium (2% glucose, 0.67% yeast nitrogen base without amino acids, 0.2% complete amino acid mixture). The stock solution was sonicated for 30 min (AS3120, Autoscience, China) and subsequently diluted in SC medium to obtain the appropriate concentrations.

2.3. Strains and growth conditions

Pichia pastoris strain GS115 (*his*$^-$ *Mut*$^+$) used in this study was obtained from Invitrogen (San Diego, CA USA). The two mutant strains, *spt23*Δ and *fad12*Δ were constructed in our previous studies (Yu et al., 2012a, 2012b). Cells were grown in liquid SC medium at 30 °C.

2.4. Growth inhibition assays

Overnight cultured cells were suspended in fresh SC liquid medium to OD_{600}=0.1. Equal volume of cell suspension and prepared GO solutions with different concentrations (0, 250, 500, 1000, 2000, 4000 ppm) were mixed in glass tubes. The mixtures were cultured at 30 °C with stirring at 180 rpm for 12 h or 24 h. The cell number in each treatment group was counted using a hemocytometer. The percent of growth was defined as the cell number divided by that of the control without GO treatment × 100.

2.5. Cell death assays

In order to evaluate the cell death, yeast cells were treated with different concentrations of GO for 24 h, harvested and suspended in PBS buffer. The cell suspensions were stained with 10 μg/mL propidium iodide (PI, prepared in distilled water, Sigma, USA) for 5 min. After staining, the cells were observed and photographed with a fluorescence microscope (BX-51, Olympus, Japan). The numbers of PI-stained cells and total cells were counted and the percentage of PI-positive cells (dead cells) was calculated as below. The percentage of death cells=(the number of PI-positive cells/the number of total cells) × 100. At least 40 fields were determined.

2.6. Cellular ROS level detection

Cellular ROS levels were measured using the 2′,7′-dichlorofluorescein diacetate (DCFH-DA) –staining method. Cells with 24 h co-incubation with GO were harvested, washed and suspended in PBS buffer. The suspensions were then stained with 10 μg/mL DCFH-DA (dissolved in ethanol, Sigma, USA) at 30 °C for 30 min. Then the cells were washed twice and resuspended in PBS buffer. The fluorescence density (FLU) was examined by a fluorescence microplate reader (PerkinElmer, USA) and the cell numbers of each treatment were calculated with a hemocytometer.

2.7. Lipid analysis

Cells were treated with different concentrations of GO, harvested and washed in distilled water. Cellular total fatty acids were extracted and methyl esterified as previously described (Yu et al., 2012a). Briefly, dry yeast powder was incubated in 5 mL 5% (w/v) KOH/methanol for saponification at 70 °C for 5 h. After the pH was adjusted to 2.0 with HCl, total fatty acids were subjected to methyl esterification with 4 mL 14% (w/v) boron trifluoride in methanol at 70 °C for 1.5 h. Then, fatty acid methyl esters (FAMEs) were extracted with *n*-hexane after addition of saturated sodium chloride solution. The FAMEs were analyzed by gas chromatography using a GC-6890 (Agilent, USA) equipped with a flame ionization detector and a HP-INNOWAX capillary column (25.0 m × 0.53 mm × 0.20 μm). The temperatures of the injector and detector were 280 °C, respectively. The oven temperature was programmed starting at 160 °C, and then increased to 210 °C at a rate of 10 °C/min, held for 5 min, and then increased gradually to 240 °C at a rate of 2 °C/min, held for 15 min. Ultra-high purity N_2 was used as the carrier gas at a constant flow rate of 1.0 mL/min. The split ratio was 4:1, and the injection volume was 5 μL. Relevant FAMEs were identified by comparison of their peaks with those of standards (Cayman Chemicals, USA).

2.8. RNA extraction and Real-time PCR

Cells were treated with GO, harvested and washed. Total RNA was extracted and used for reverse transcriptional synthesis of cDNA as previously described (Yu et al., 2014). Real-time PCR was performed using SYBR Green qPCR Supermix (TransGen Biotech) according to the instructions. The transcriptional levels of the genes, *FAD9A*, *FAD9B*, *FAD12*, *FAD15* and *SPT23*, were normalized against the levels of *ACT1* gene in different samples. Primers used in the assay are listed in Table 1. All the results were performed in triplicate and repeated in three independent experiments.

2.9. Statistical analysis

Each experiment was performed with three replicates, and the value represents the mean ± standard deviation of three experiments. Significant differences between the treatments were determined using one-way ANOVA ($P < 0.05$). All statistical analyses were performed by Statistical Packages for the Social Sciences (SPSS, Version 20).

3. Results

3.1. Characterization of the synthesized GO

When examined by TEM, the synthesized GO showed thin films

Table 1
Primers used in this study.

Primer	Sequences (5′-3′)
PPACT-F	GGTTCCCACTTATTTCCCAG
PPACT-R	TCCTTCAGTTTTTCCGTCTC
PPD9-F	GAGACCCTCATAACATCCGA
PPD9-R	CAGTCCACCATAAACAAGCC
PPD9B-F	CCAAGATACAAGGCAAGAGC
PPD9B-R	CACCGTAGATAAATCCACCC
PPD12-F	CCTACCCCAACACCCCTAAA
PPD12-R	CAACTGTGCCAAGATACCCA
PPD15-F	TCCTCTCCTGTTTTTGATAA
PPD15-R	GGACGAGTCTGTGTGTTGTA
REAL-SPT23-F	ATCAATCCAGTCACGCCTC
REAL-SPT23-R	TGTAGTGGGCATTCTGAGC

of few layers (Fig. 1a). Raman spectroscopy further revealed that the GO had the two characteristic bands (1350 cm^{-1} and 1580 cm^{-1}) (Fig. 1b), which are attributed to the local defects at the edge of GO and the sp^2 graphitized structure.

3.2. Toxicity of the synthesized GO toward Pichia pastoris

We tested the effect of GO on the growth of yeast cells. The synthesized GO showed dose-dependent toxicity to *P. pastoris*. As shown in Fig. 2a, after incubated for 24 h, the GO at 0–250 ppm had no obvious influence on cell growth. When the concentrations were higher than 500 ppm, it showed significant inhibition activity against cell growth, leading to significant decrease of growth biomass ($IC_{50}=1125\pm40$ ppm). Moreover, the difference among the relative growth rates under different concentration of GO treatments demonstrated that high concentration of GO ($\geq$ 1000 ppm) impact cell proliferation (Fig. 2b).

We further investigated whether the growth inhibition was associated with cell membrane damage. We used PI to measure the membrane damage levels. The results showed that only $\geq$ 500 ppm of GO caused remarkably increased PI-positive cell numbers (Fig. 2c). To demonstrated our speculation, we used TEM to characterize the ultrastructural PM changes after treatment of 500 ppm GO for 24 h (Fig. 2d and e). Compared with the control group, the PM showed distinct disruption, indicating strong PM damage after GO treatment. It is suggested that the dose-dependent toxicity to *P. pastoris* was due to the cell membrane damage when the concentration of GO was above 500 ppm.

3.3. GO caused increased ROS under high concentrations

As GO led to membrane damage, we further investigated whether the nanomaterials could cause intracellular damage, such as ROS accumulation. The increased ROS levels could overwhelm the cellular antioxidant defense system and lead to oxidative stress (Ray et al., 2012). It results in direct or indirect ROS-mediated damage to biomolecules such as nucleic acids, proteins, structural carbohydrates and lipids (Catala, 2012). DCFH-DA staining was used to determine ROS levels. The results showed that $\geq$ 1000 ppm of GO led to significant increase of intracellular ROS levels, while 250–500 ppm not (Fig. 3). These results suggested that when the concentrations of GO were higher than 1000 ppm, membrane damage and oxidative damage played important roles in the toxicity to *P. pastoris* together.

3.4. GO changed cellular fatty acid profiles

It is known that the physical property of membrane is associated with fatty acids, especially unsaturated fatty acids (UFAs). As the cells can overcome the membrane damage of GO at $\leq$ 500 ppm, we proposed that the relative contents of cellular UFAs may change to alleviate membrane damage. Therefore, we treated the cells with different concentrations of GO (0, 250, 500, 1000, 2000 ppm), extracted cellular fatty acids and measured the relative abundance of the corresponding fatty acid products using the GC method (Fig. 4). Unexpectedly, there was no obvious change in the unsaturated level among the cultured conditions (Fig. 4a). Interestingly, we noticed that cellular UFA profiles were changed (Fig. 4b). The relative contents of saturated fatty acid (SFAs), including palmitic acid (PA, 16:0) and stearic acid (SA, 18:0), remained unchanged. In contrast, the relative contents of each UFA were altered: the contents of monounsaturated fatty acid (MUFA) oleic acid (OA, 18:1) decreased, while the contents of polyunsaturated fatty acids (PUFAs) linoleic acid (LA, 18:2) and α-linolenic acid (ALA, 18:3) increased. Hence, although the unsaturated levels remained the same, cellular fatty acid profiles changed. It seemed to be related to the alleviation of cell damage caused by GO addition.

3.5. GO up-regulated the expression of UFA synthesis-related genes

As demonstrated above, GO treatment caused a change of cellular UFA profiles. Further, we focused on the mechanisms of increase in PUFAs synthesis. In *P. pastoris*, four desaturase genes are in charge of UFAs synthesis, including *FAD9A* and *FAD9B* (encoding

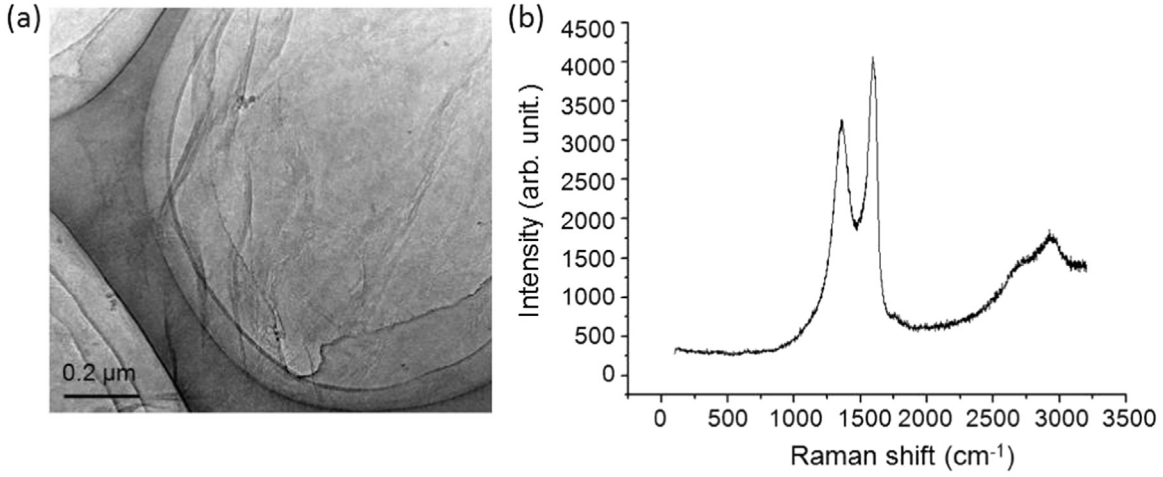

Fig. 1. Characterization of the synthesized GO. (a) TEM observation of the synthesized GO. (b) Raman spectroscopy of the GO.

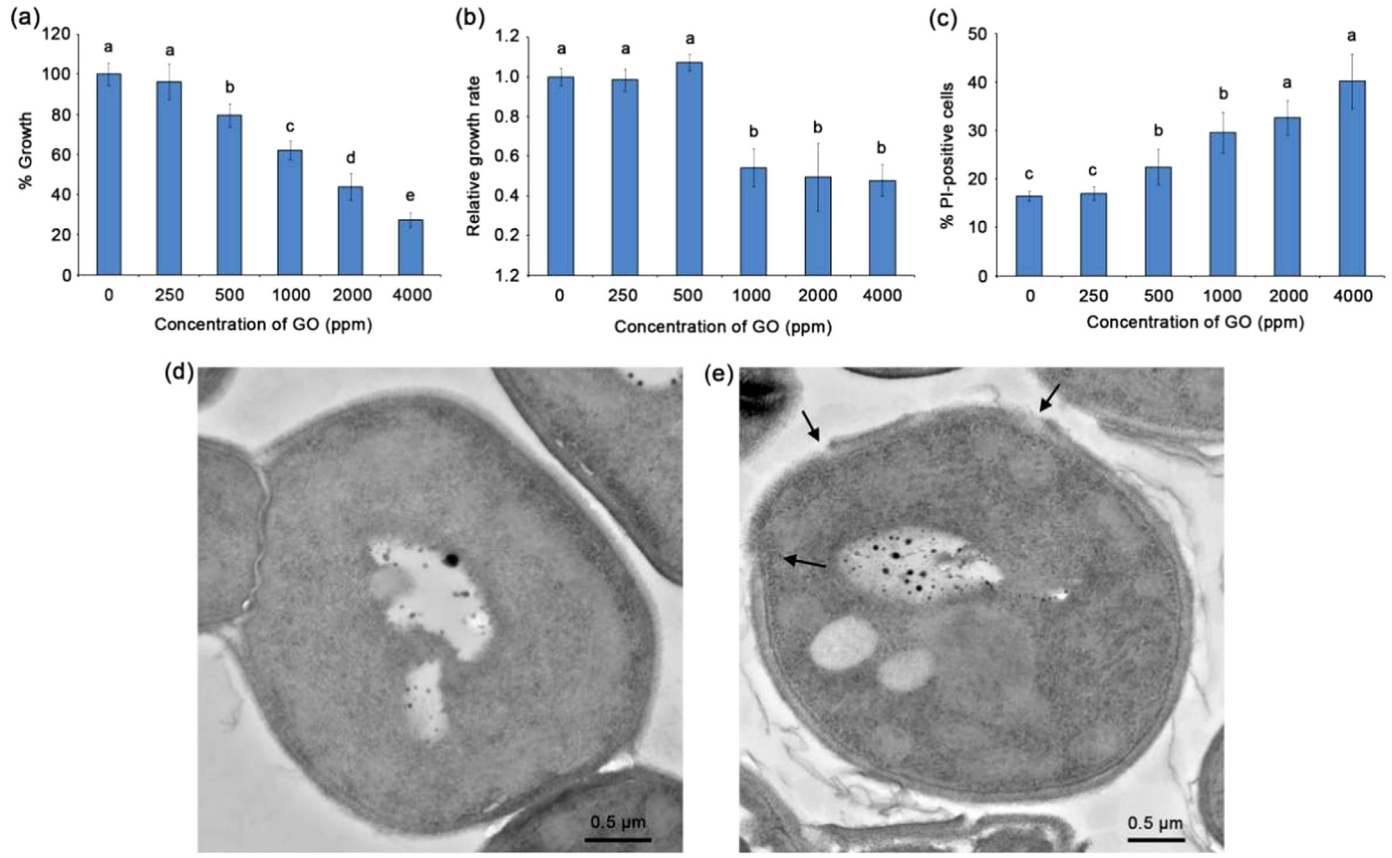

Fig. 2. Growth inhibition and toxicity of the synthesized GO to *P. pastoris*. (a) The yeast cells were co-incubated with different concentrations of GO for 24 h and counted. The percent of growth in each group was calculated as the cell number of each group divided by that of the control × 100. (b) The yeast cells were co-incubated with different concentrations of GO. The cell number of each group was counted during the exponential growth phase at 12 h and 16 h, respectively. The growth rate was calculated by the cell number difference between 12 h and 16 h divided by cultured duration (4 h). The relative growth rate was normalized with the value of 0 ppm. (c) The treated cells were stained with PI and observed by fluorescence microscopy. The percent of PI-positive cells was calculated by the number of PI-positive cells divided by that of total cells × 100. (d) and (e) Ultrastructure of the yeast cells cultured in SC (d) or SC plus 500 ppm GO (e). The arrows indicate the damage of plasma membrane. Scale bar = 0.5 μm. The values represent the means ± standard deviation. Identical letters indicate no statistical differences among the treatments ($P < 0.05$).

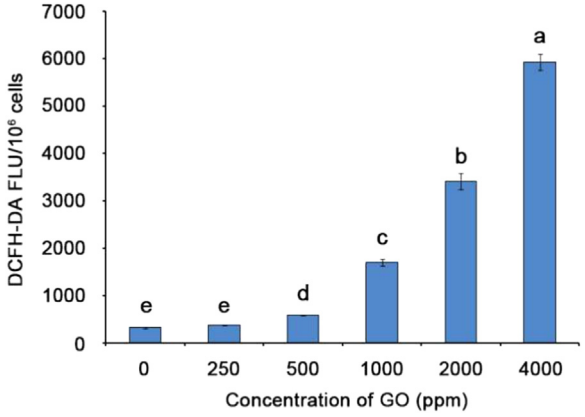

Fig. 3. Cellular ROS levels with different concentrations of GO treatments. Cells were treated with different concentrations of GO and stained with DCFH-DA for 30 min, and the fluorescence intensities were determined. Error bars correspond to the SD calculated from three repeated experiments. The values represent the means ± standard deviation. Identical letters indicate no statistical differences among the treatments ($P < 0.05$).

Δ-9 desaturase), *FAD12* (encoding Δ-12 desaturase) and *FAD15* (encoding Δ-15 desaturase) (Yu et al., 2012b). All of the desaturase genes are regulated by the transcriptional factor Spt23 (Yu et al., 2012a). As shown in Fig. 5, *FAD9A*, *FAD9B* and *FAD12* were remarkably up-regulated and *FAD12* changed more distinctly under the treatment of GO. These results revealed that when cells were exposed to GO, *FAD12* was primarily activated which led to the following increase of PUFA contents.

3.6. UFAs play critical roles in defending GO damages

As above showed that cellular UFA contents changed when treated with GO, we wondered if UFA defective strains would show growth inhibition by GO treatment. Two UFA synthesis mutant strains, *spt23*Δ and *fad12*Δ, were cultured with 500 ppm GO and growth situations were measured. The mutant strain *spt23*Δ has a defect in OA synthesis and *fad12*Δ fails in LA and ALA synthesis (Yu et al., 2012a, 2012b). As shown in Fig. 6a, the growth of *fad12*Δ was inhibited by GO severely on either 12 h or 24 h. This suggested that the synthesis of LA and ALA was important to overcome the GO damage. Meanwhile, we used PI-staining to observe the mortality of each strain. On the contrast, *spt23*Δ showed the highest death rate among the three strains. It is possible that MUFA and PUFA play different roles on cell survival mechanism against GO treatment.

4. Discussion

Graphene is a rapidly rising star in the aspect of material science and condensed-matter physics (Geim and Novoselov, 2007). Due to its unique physical and chemical character, graphene is potentially utilized for a variety of applications, especially

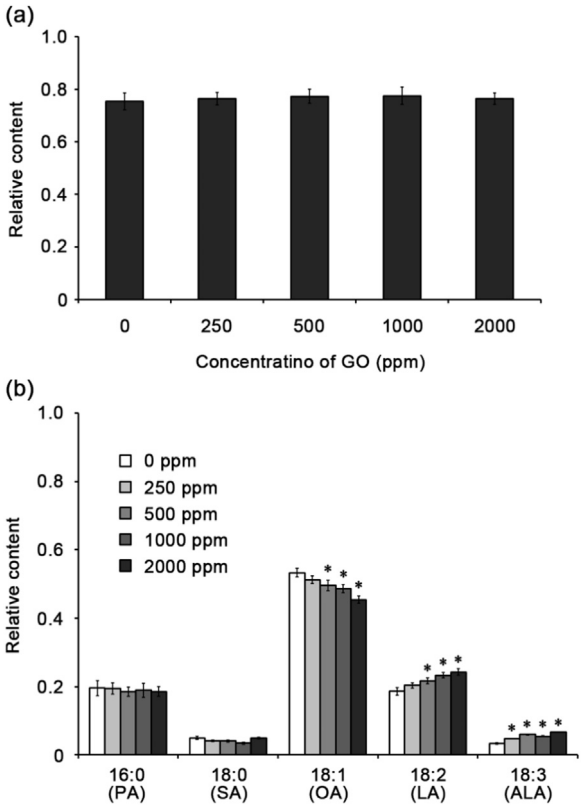

Fig. 4. Effect of GO on cellular fatty acid profiles. Cells were treated with different concentrations of GO (0, 250, 500, 1000 and 2000 ppm) for 24 h and fatty acids were extracted for GC analysis. Unsaturated levels (a) and fatty acid profiles (b) were calculated. The values represent the means ± standard deviation. Asterisks denote statistical significance between the treated cells and the control cells ($P < 0.05$).

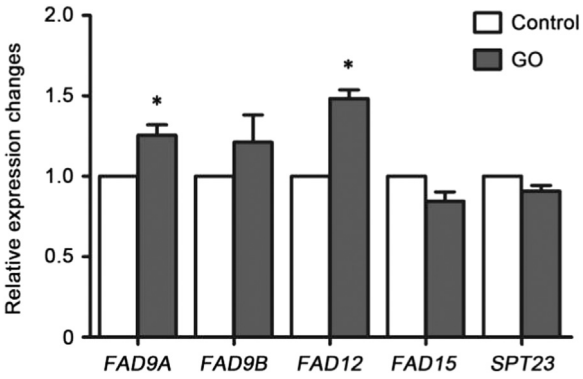

Fig. 5. Effect of GO on the mRNA levels of UFA synthesis-related genes. Yeast cells were treated with or without 500 ppm GO for 24 h and the mRNA expression levels of *FAD9A*, *FAD9B*, *FAD12*, *FAD15* and *SPT23* were measured. The values represent the means ± standard deviation. Asterisks denote statistical significance between the treated cells and the control cells ($P < 0.05$).

biomedical applications. Prior to using the material for a series of biomedical applications, its biological safety should be noted. In this study, we found that graphene oxide had a low toxicity to the industrial fungus, *P. pastoris*, mainly owing to membrane damage and ROS accumulation. Exposure to GO could regulate the cellular UFA profiles in order to overcome the adverse situation. Taken together, these results demonstrate that UFAs, especially PUFAs, play a vital role in resisting GO damage in *Pichia pastoris*.

Recent studies have shown that GO exhibits cytotoxicity toward a variety of organisms, mainly including mammalian cells (Akhavan et al., 2015; Duan et al., 2015; Liao et al., 2011) and bacteria (Gurunathan, 2015; Tu et al., 2013). However, there are few reported studies described to reveal the toxicity and toxicology to eukaryotic microorganisms, especially yeast cells. GO influences cell viability in mainly two ways, including membrane damage and oxidative stress. An experiment suggested that GO could induce the degradation of the inner and outer cell membranes of *Escherichia coli* by extracting large amounts of phospholipids from the cell membranes (Tu et al., 2013). Besides, oxidative stress is another important cell damage factor by ROS accumulation or direct oxidation of cellular components (Romero-Vargas Castrillón et al., 2015).

In this study, we first prepared GO solutions and tested its toxicity to the industry organism *Pichia pastoris*. We found that low concentrations of GO did not cause cell death. The cell viability decreased with the increase of concentrations and the concentration effect of inflection was 500 ppm. Further, when the cells were exposed to high concentrations of GO, the number of PI-positive cells increased and cellular ROS accumulated remarkably. This suggested that GO causes cytotoxicity in high concentration. As an extraneous matter, when added into cell culture, GO may trigger cell damage including membrane damage and ROS accumulation. As is well-known, although ROS functions as signaling molecules in maintaining life activities, it has been shown to be toxic (D'Autréaux and Toledano, 2007). There are many cell death processes associated with excess ROS accumulation. Simultaneously, broken cell membrane may further promote cell death.

UFAs are involved in many cell functions because they are important components in cell membrane lipids and cellular storage lipids in all eukaryotes. In our study, we found that exposure to GO led to a change in UFA profiles that MUFA (OA) decreased while PUFAs (LA and ALA) increased. As is known, the number of double bonds in fatty acids determines the physical properties of cell membrane. Further, the nature of the plasma membrane is an important parameter to estimate the cell survival ability to environmental disturbance. When cells were against with GO, it may trigger cell protection process, which involved the change of cellular fatty acids. According to this study, the increased PUFAs meant more double bonds which could be incorporated into membrane lipids. Consequently, the nature of the plasma membrane changed and the cells could better adapt to the external environment.

In order to verify our hypothesis, two UFA synthesis defective strains, *spt23*Δ and *fad12*Δ, were cultured in the medium plus GO. In our previous study, we demonstrated that deletion of *SPT23* led to distinctly decreased OA production and deletion of *FAD12* led to the absence of LA and ALA in *Pichia pastoris* (Yu et al., 2012a, 2012b). The results showed that GO inhibited the growth of *fad12*Δ seriously while *spt23*Δ was easier to die. It is suggested that loss of LA and ALA may lead to decreased ability of GO damage resistance which just coincided with the results above that GO treatment increased cellular contents of LA and ALA. Hence, PUFAs are critical for cell survival against GO. In addition, the mutant strain *spt23*Δ showed a high death rate while a low growth inhibition rate. We speculated that since *spt23*Δ could produce the normal levels of LA and ALA, but OA, deletion of *SPT23* only influenced its viability without growth inhibition upon GO treatment.

Considering the difference between MUFA and PUFA in response to GO attack, we hypothesized the various desaturases may be affected differentially by GO due to their different location. Generally, the first double bond introduction by Δ-9 desaturase occurs in the cytosol and subsequent desaturation takes place after C18:1 esterification with a phospholipid in the endoplasmic reticulum (Bellou et al., 2016; Certik and Shimizu, 1999). Since extracellular GO caused PM damage, it suggested that GO may attack other cellular membrane system. Hence, the desaturases located in

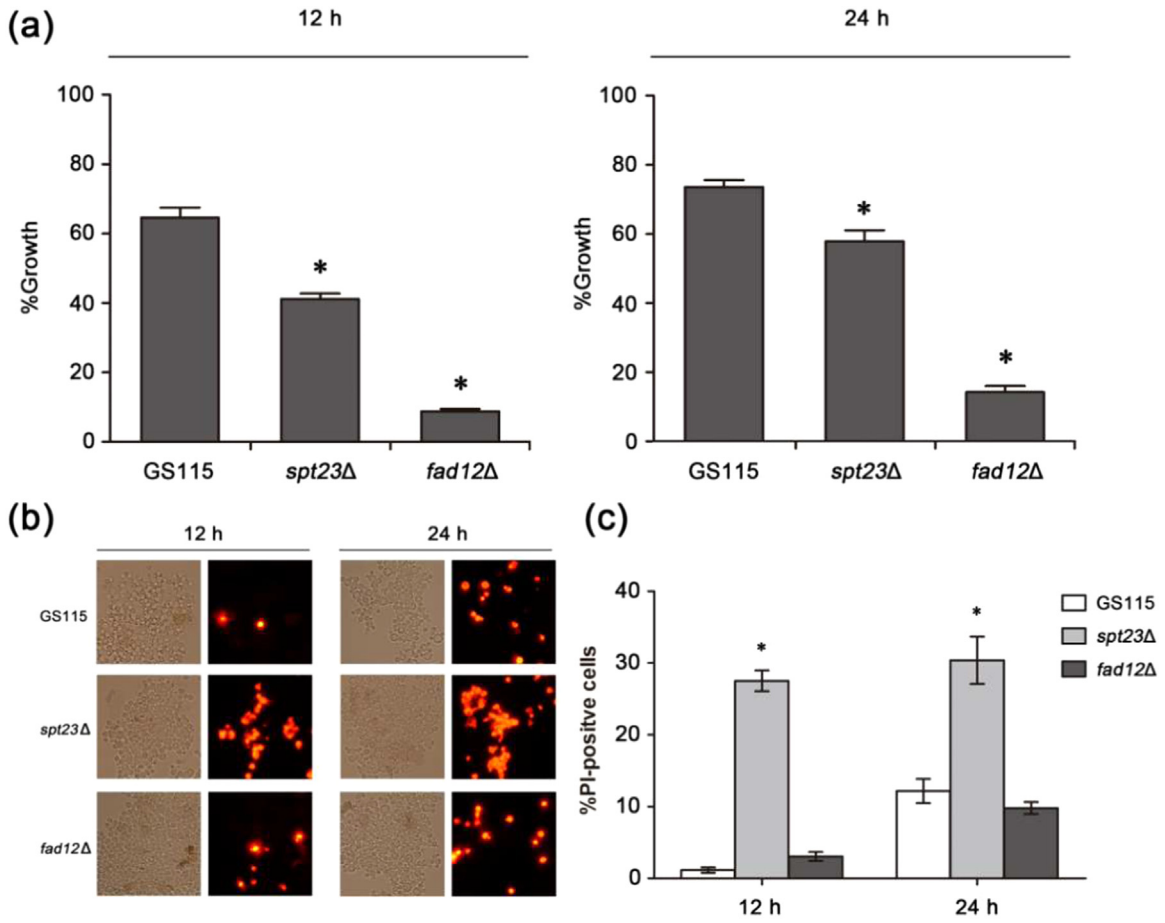

Fig. 6. UFAs play critical roles in defending GO damages and cell survival. (a) The wild-type strain GS115 and the two mutant strains, *spt23*Δ and *fad12*Δ, were cultured with 500 ppm GO for 12 h or 24 h. The percent of growth in each group was calculated as the cell number of each treated group divided by that of the control × 100. (b) The treated cells were stained with PI and observed by fluorescence microscopy. The percent of PI-positive cells was calculated by the number of PI-positive cells divided by that of total cells × 100. The values represent the means ± standard deviation. Identical letters indicate no statistical differences among the treatments ($P < 0.05$).

the endoplasmic reticulum may play a dominant role in the defense mechanism.

According to the differences in cellular fatty acid composition under GO treatment, we further considered the impact on phospholipids (PLs) given by GO addition. PLs are important components of biological membranes and are important precursors of signaling molecules (Vance and Vance, 2005). The fatty acyl composition of PLs determines the biophysical characteristics of membranes (Spector and Yorek, 1985). Membrane fluidity can be impacted by increased fatty acid saturation. The relative quantity of saturated and unsaturated acyl chains affects membrane fluidity and thickness (van Meer et al., 2008). Co-culture with GO increased the PUFAs contents which may affect the PLs fatty acyl composition. Introduction of more double bonds of membrane lipids alter their conformation and influence physical properties of the membranes (Los and Murata, 2004). It has been demonstrated

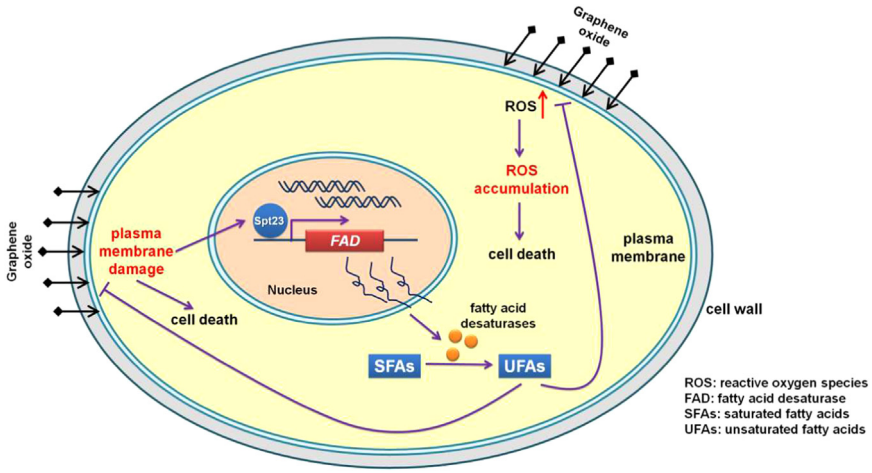

Fig. 7. A simple model for interaction between GO and *Pichia pastoris*.

polyunsaturated PLs make pure lipid bilayers more flexible (Rawicz et al., 2000). When more PUFAs were incorporated into PLs, the plasma membrane became more amenable to deformation which suggested polyunsaturated PLs may help to support endocytosis (Pinot et al., 2014). When cells were under GO threat, the expression of *FAD* genes was activated which resulted in increased content of PUFAs. Then, more PUFAs can be incorporated in PLs to promote endocytosis. We speculated that cells can transport GO from cell surface to vacuole via endocytosis so that it can be degraded for detoxification. Taken together, PUFAs (LA and ALA) were essential for cells to resist GO toxicity.

Among the cellular lipid fractions, PLs are more susceptible to oxidative stress and the nature of PLs is more important than the unsaturation level. The neutral PLs (phosphatidylcholine and phosphatidylethanolamine) are more susceptible to peroxidation than the anionic PLs (phosphatidylinositol and phosphatidylserine) (Fakas et al., 2008). We speculated that ROS accumulation had a connection with neutral PLs which reside in cytoplasmic lipid bodies rather than the increased PUFAs.

5. Conclusion

Our study demonstrated that GO had dose-dependent toxicity to *Pichia pastoris*, mainly owing to cellular ROS accumulation and plasma membrane damage. In order to get through the dilemma, gene expression of *FAD12* was distinctly activated, leading to the change of UFA profiles. A connection between membrane lipids and resistance to GO attack was then proposed (Fig. 7). Further detailed studies are required to investigate how GO interact with the cell membrane, especially membrane lipids, to figure out the relationship between UFAs and GO damage.

Acknowledgment

We thank reviewers for critical reading and helpful suggestions. This work was supported by National Natural Science Foundation of China (No. 31270096, No. 31400132).

References

Akhavan, O., et al., 2015. Dose-dependent effects of nanoscale graphene oxide on reproduction capability of mammals. Carbon 95, 309–317.
Balandin, A.A., 2011. Thermal properties of graphene and nanostructured carbon materials. Nat. Mater. 10, 569–581.
Bellou, S., et al., 2016. Microbial oils as food additives: recent approaches for improving microbial oil production and its polyunsaturated fatty acid content. Curr. Opin. Biotechnol. 37, 24–35.
Belyanskaya, L., et al., 2009. Effects of carbon nanotubes on primary neurons and glial cells. Neurotoxicology 30, 702–711.
Bunch, J.S., et al., 2008. Impermeable atomic membranes from graphene sheets. Nano Lett. 8, 2458–2462.
Carracedo, A., et al., 2013. Cancer metabolism: fatty acid oxidation in the limelight. Nat. Rev. Cancer 13, 227–232.
Catala, A., 2012. Lipid peroxidation modifies the picture of membranes from the "Fluid Mosaic Model" to the "Lipid Whisker Model". Biochimie 94, 101–109.
Certik, M., Shimizu, S., 1999. Biosynthesis and regulation of microbial polyunsaturated fatty acid production. J. Biosci. Bioeng. 87, 1–14.
D'Autréaux, B., Toledano, M.B., 2007. ROS as signalling molecules: mechanisms that generate specificity in ROS homeostasis. Nat. Rev. Mol. Cell Biol. 8, 813–824.
Duan, G., et al., 2015. Protein corona mitigates the cytotoxicity of graphene oxide by reducing its physical interaction with cell membrane. Nanoscale 7, 15214–15224.
Elias, D.C., et al., 2009. Control of graphene's properties by reversible hydrogenation: evidence for graphane. Science 323, 610–613.
Fakas, S., et al., 2008. Susceptibility to peroxidation of the major mycelial lipids of *Cunninghamella echinulata*. Eur. J. Lipid Sci. Technol. 110, 1062–1067.
Geim, A.K., Novoselov, K.S., 2007. The rise of graphene. Nat. Mater. 6, 183–191.
Gurunathan, S., 2015. Cytotoxicity of graphene oxide nanoparticles on plant growth promoting rhizobacteria. J. Ind. Eng. Chem. 32, 282–291.
Hirano, S., et al., 2008. Multi-walled carbon nanotubes injure the plasma membrane of macrophages. Toxicol. Appl. Pharmacol. 232, 244–251.
Hummers Jr, W.S., Offeman, R.E., 1958. Preparation of graphitic oxide. J. Am. Chem. Soc. 80 1339–1339.
Li, Y., et al., 2012. The triggering of apoptosis in macrophages by pristine graphene through the MAPK and TGF-beta signaling pathways. Biomaterials 33, 402–411.
Liao, K.H., et al., 2011. Cytotoxicity of graphene oxide and graphene in human erythrocytes and skin fibroblasts. ACS Appl. Mater. Interfaces 3, 2607–2615.
Los, D.A., Murata, N., 2004. Membrane fluidity and its roles in the perception of environmental signals. Biochim. Biophys. Acta 1666, 142–157.
Mayorov, A.S., et al., 2011. Micrometer-scale ballistic transport in encapsulated graphene at room temperature. Nano Lett. 11, 2396–2399.
Murray, A.R., et al., 2009. Oxidative stress and inflammatory response in dermal toxicity of single-walled carbon nanotubes. Toxicology 257, 161–171.
Nair, R.R., et al., 2008. Fine structure constant defines visual transparency of graphene. Science 320, 1308.
Nair, R.R., et al., 2010. Fluorographene: a two-dimensional counterpart of Teflon. Small 6, 2877–2884.
Novoselov, K.S., et al., 2012. A roadmap for graphene. Nature 490, 192–200.
Pinot, M., et al., 2014. Lipid cell biology. Polyunsaturated phospholipids facilitate membrane deformation and fission by endocytic proteins. Science 345, 693–697.
Rawicz, W., et al., 2000. Effect of chain length and unsaturation on elasticity of lipid bilayers. Biophys. J. 79, 328–339.
Ray, P.D., et al., 2012. Reactive oxygen species (ROS) homeostasis and redox regulation in cellular signaling. Cell Signal. 24, 981–990.
Romero-Vargas Castrillón, S., et al., 2015. Interaction of graphene oxide with bacterial cell membranes: insights from force spectroscopy. Environ. Sci. Technol. Lett. 2, 112–117.
Spector, A.A., Yorek, M.A., 1985. Membrane lipid composition and cellular function. J. Lipid Res. 26, 1015–1035.
Tu, Y., et al., 2013. Destructive extraction of phospholipids from *Escherichia coli* membranes by graphene nanosheets. Nat. Nanotechnol. 8, 594–601.
van Meer, G., et al., 2008. Membrane lipids: where they are and how they behave. Nat. Rev. Mol. Cell Biol. 9, 112–124.
Vance, J.E., Vance, D.E., 2005. Metabolic insights into phospholipid function using gene-targeted mice. J. Biol. Chem. 280, 10877–10880.
Yu, A.Q., et al., 2012a. Transcriptional regulation of desaturase genes in Pichia pastoris GS115. Lipids 47, 1099–1108.
Yu, A.Q., et al., 2012b. Knockout of fatty acid desaturase genes in Pichia pastoris GS115 and its effect on the fatty acid biosynthesis and physiological consequences. Arch. Microbiol. 194, 1023–1032.
Yu, Q., et al., 2014. A novel role of the vacuolar calcium channel Yvc1 in stress response, morphogenesis and pathogenicity of *Candida albicans*. Int. J. Med. Microbiol. 304, 339–350.
Zhang, Y., et al., 2014. Toxicity and efficacy of carbon nanotubes and graphene: the utility of carbon-based nanoparticles in nanomedicine. Drug Metab. Rev. 46, 232–246.